Molecular Recognition in an Organic Host–Guest Complex: CH···O and CH···π Interactions Completely Control the Crystal Packing and the Host–Guest Complexation

Kokkuvayil Vasu Radhakrishnan,[*1] **Saithalavi Anas,**[1] **Eringathodi Suresh,**[2]
Nobuaki Koga,[3] **and Cherumuttathu Hariharan Suresh**[*4]

[1]Organic Chemistry Section, Regional Research Laboratory (CSIR), Trivandrum 695 019, India

[2]Analytical Sciences Discipline, Central Salt and Marine Chemicals Research Institute, Bhavnagar-364 002, Gujarat, India

[3]Graduate School of Information Science, Nagoya University, Nagoya 464-8601

[4]Computational Modeling and Simulation Section, Regional Research Laboratory (CSIR), Trivandrum 695 019, India

Received September 1, 2006; E-mail: sureshch@gmail.com

The synthesis, crystal structure analysis, theoretical modeling at DFT and semiempirical PM3 levels, and molecular electrostatic potential analysis of an organic host–guest system containing an azapolycyclic system **3** and ethyl acetate are presented. The structure of **3** was charaterized by the presence of seven-connected five-membered rings. Though **3** contained six-saturated nitrogen atoms capable of CH···N interactions, its crystal structure and the host–guest complexation were completely governed by CH···O and CH···π interactions. Further, an aromatic pocket consisting of four phenyl rings from four molecules of **3** existed located in the crystal structure. The guest molecule ethyl acetate trapped inside this aromatic pocket was found to interact with it via three CH···π and two CH···O interactions. A model structure for this host–guest complex was also optimized at DFT level, which showed good agreement with the experimental structure.

Results and Discussion

Several chemical and biochemical processes are initiated when a molecule is recognized by another molecule via specific intermolecular interactions.[1] Among these interactions, hydrogen bonding is considered as one of the most important interaction types.[2] Several categories of hydrogen bonding are observed in nature which range from the very strong (168 kJ mol^{-1}) to very weak (1.05 kJ mol^{-1}).[1b,3] Weak interactions, such as CH···O and CH···π, which are in the range from 21 to 4.2 kJ mol^{-1} are becoming increasingly important in crystal engineering, protein folding studies, enzyme action in biology and in host–guest chemistry.[4] The CH···O type interaction has been suggested to be a prototype of a X–H···A hydrogen bond, where X and A have moderate to low electronegativity. The attraction between the CH bond and a π system is generally termed as the CH···π interaction. Using the Cambridge crystallographic structural database, Nishio and co-workers demonstrated that the CH···π interaction plays an appreciable role in controlling the conformation of organic molecules in their crystals.[5] Several recent findings on CH···π interactions shown their importance in understanding a variety of molecular phenomena.[6] In this work, we report an organic host–guest system which is rich in CH···O and CH···π interactions. The details of its synthesis, crystal structure analysis, theoretical modeling at DFT and semiempirical PM3 levels, and molecular electrostatic potential analysis are presented.

Results and Discussion

Synthesis and Crystal Strcuture Analysis of Azapolycycle 3. Our investigations involved the reaction of 4-phenyl-3*H*-1,2,4-triazole-3,5(4*H*)-dione with 6,6-diphenyl fulvene.[7a] Pentafulvenes are an important class of organic compounds and have been used as an important synthon in synthetic organic chemistry.[7b] Fulvenes act as a 2π, 4π, or 6π component in its cycloaddition with various partners.[8] 4-Substituted-3*H*-1,2,4-triazole-3,5(4*H*)-dione is a reactive dienophile; it undergoes smooth Diels–Alder reaction with dienes[9] and ene reaction[10] with olefins. Compound **3** was synthesized via the reaction of 6,6-diphenylfulvene (**1**) with 4-phenyl-3*H*-1,2,4-triazole-3,5(4*H*)-dione (**2**). The reaction proceeded smoothly affording a mixture of azapolycycles **3** and **4** in 81% yield (Scheme 1).

The structures were assigned to the products **3** and **4** based on spectral analysis and by comparison to the literature.[7a] Further, the structure of **3** was unambiguously confirmed by single-crystal X-ray analysis (Fig. 1).[11] Compound **3** is structurally and electronically very interesting because it consists of a network of seven-connected five-membered rings containing six-saturated nitrogen atoms with lone-pair electrons, four C=O bonds, and six phenyl rings. Therefore, interesting intermolecular interactions are expected in this system.

In an attempt to understand the various molecular interactions, we analyzed the detailed packing mode and hydrogen-bonding interactions of compound **3**. The analysis showed the formation of a well-defined dimeric unit in the crystal of **3** (Fig. 2). As we can see from Fig. 2, two azapolycyclic ligands aligned in such a way that hydrogen-bonded dimers formrd through CH···O interactions from one oxygen atom from each dihydrotriazole dione moiety present in the mole-
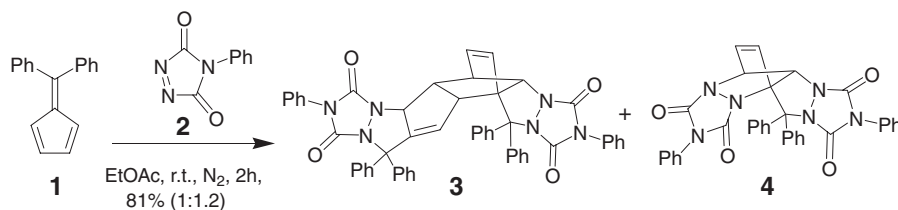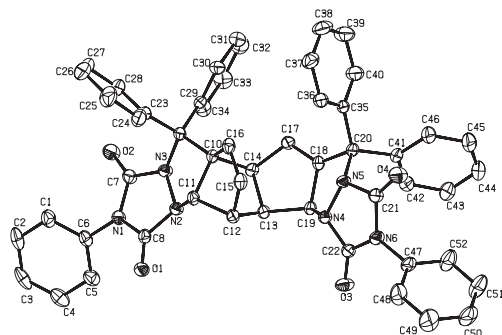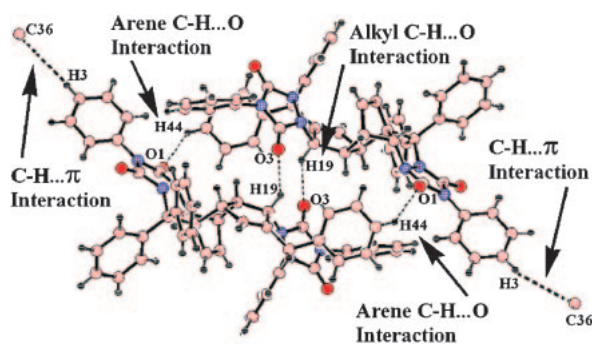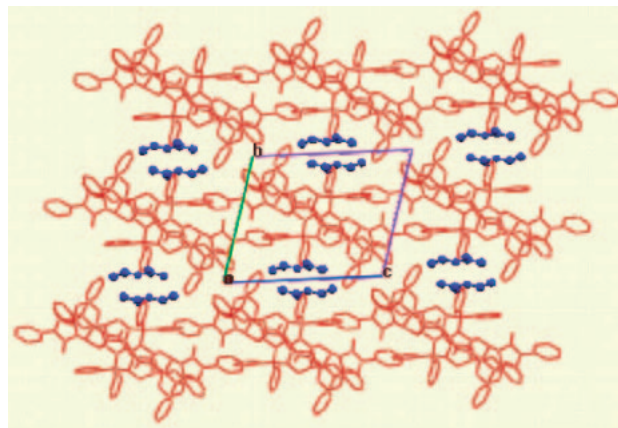
Scheme 1.

Fig. 1.   ORTEP diagram of **3**.

Fig. 2.   The dimeric molecular association between the aza-polycyclic ligand via CH⋯O interactions (hydrogen-bonding interactions are shown as dotted lines).

Fig. 3.   Packing diagram of the compound viewed down *a*-axis showing the arrangement of the organic moiety (red) with ethyl acetate molecule (blue, ball and stick model) in the crystal lattice. H-atoms are omitted for clarity.
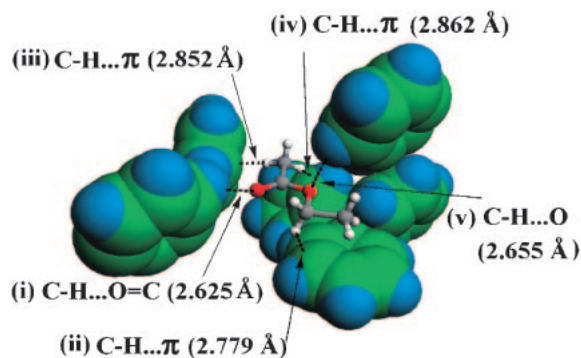
Fig. 4.   The ethyl acetate molecule and the surrounding phenyl groups. The phenyl groups in the interactions labeled as (i), (ii), (iii), and (v) belong to different molecules of **3**. Interaction (iv) corresponds to the π bond of the five-membered carbon cycle and the alkyl CH bond.

cule. Hydrogen bonding in the dimer essentially involves the phenyl hydrogen atom with the dione oxygen, and alkyl hydrogen atom from the central five-membered ring with the dione oxygens. The various hydrogen-bonding interaction parameters with the symmetry code are H44⋯O1 = 2.543 Å; ∠C44–H44⋯O1 = 120°; H19⋯O3 = 2.369 Å, ∠C19–H19⋯O3 = 137° (symmetry code $1 - x$, $1 - y$, $1 - z$). These hydrogen-bonded dimers were further arranged as bilayers via CH⋯π interactions with the neighboring dimeric units extending along *c*-axis. The parameters for CH⋯π interactions are H3⋯C36 = 2.836 Å and ∠C3–H3⋯C36 = 161°.

Figure 3 depicts the packing diagram of the compound viewed down *a*-axis. Interestingly, the ethyl acetate molecules were occupied between the neighboring bilayers of the aza-polycyclic moieties creating alternate layers of the host–guest system along *bc*-plane. A close look at the region around ethyl acetate revealed the formation of an aromatic pocket containing four phenyl rings from four molecules of **3**. Ethyl acetate molecules are held in the aromatic pocket by three alkyl CH⋯π, one CH⋯O=C, and another bifurcated CH⋯O interaction between the oxygen atoms from the ethyl acetate molecule

with the phenyl hydrogen from the organic ligand. These interactions are depicted in Fig. 4 along with the corresponding interaction distances. The CH⋯π interaction (iv), depicted in Fig. 4, corresponds to the interaction between the CH bond of acetate moiety and the π bond in the five-membered carbocycle. The other two CH⋯π interactions ((ii) and (iii)) correspond to arene CH⋯π interactions. Mainly the collective strength of the five interactions shown in Fig. 4 holds and stabilies the guest molecule in the crystal lattice.

Theoretical Modeling.   The molecular geometries were optimized at the DFT level by using the Becke's three-parameter exchange functional (B3)[12] in conjunction with the Lee–Yang–Parr correlation functional (LYP)[13] as implemented in
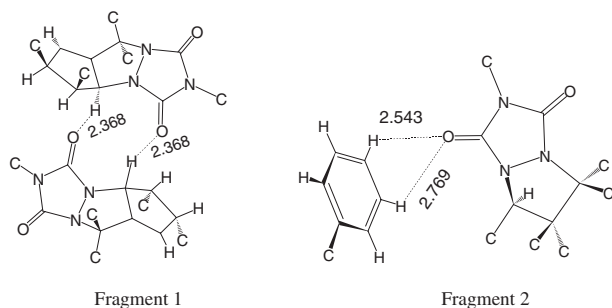
Fig. 5.   Fragment structures taken from the dimer showing the main hydrogen-bonding interactions (distances in Å).

the Gaussian 03 suite of programs.[14] This method known as B3LYP was used along with 6-31G* basis functions selected for H, C, N, and O.[15] For interaction energy calculations, single point energy calculations were done using the B3LYP/6-311++G(d,p) level of theory. However, for molecular assemblies containing four molecules of **3** and ethyl acetate (total 414 atoms), PM3 level of semiempirical method was used for the geometry optimization.[16] Gaussian 03 program was also employed for calculating the molecular electrostatic potential (MESP) at B3LYP/6-31G* level. For a molecule with positive nuclear charge $\{Z_A\}$ located at nuclear positive vectors $\{R_A\}$ and electron density $\rho(r)$ distribution at all points in space, the MESP, $V(r)$(in au) is given by[17a,b]

$$V(r) = \sum_{A}^{N} \frac{Z_A}{|r - R_A|} - \int \frac{\rho(r')d^3r'}{|r - r'|}. \quad (1)$$

Equation 1 is also interpreted as the work done in bringing a unit test positive charge from infinity to a point of reference in the vicinity of the molecule. It should be noted that MESP is a real physical property of a molecule and can be determined experimentally by X-ray diffraction techniques. This quantity is used widely for understanding molecular reactivity, intermolecular interactions, molecular recognition, electrophilic reactions, and a variety of chemical phenomena.[17] Visualization of MESP is a good way to see the charge distribution within a molecule. Local minima of MESP is often observed at the lone pair region of a molecule because of the larger value of the electronic term in Eq. 1 (second term) as compared to the bare nuclear term and these points generally represented centers of negative charge on the molecule.[17b]

The dimer of **3** and even **3** itself were quite big for doing an accurate quantum chemical calculation at reasonable computational cost. Therefore, in order to gain a deeper understanding of the molecular recognition phenomenon and to evaluate the energetic stabilization of CH⋯O and CH⋯π interactions, model molecules were used in the calculations.

The fragments containing the major interaction in the dimer are presented in Fig. 5. The model systems (Model A and Model B) were made from these fragments by replacing the atoms with insufficient valency by hydrogen atoms. These structures optimized at B3LYP/6-31G* level are presented in Fig. 6. CH⋯O hydrogen-bond interactions were clearly observed in Model A and B (depicted in the Fig. 6 as gray lines). In Model A, a hydrogen-bond distance was 2.530 Å for the alkyl CH⋯O interaction, which is 0.162 Å longer than the value
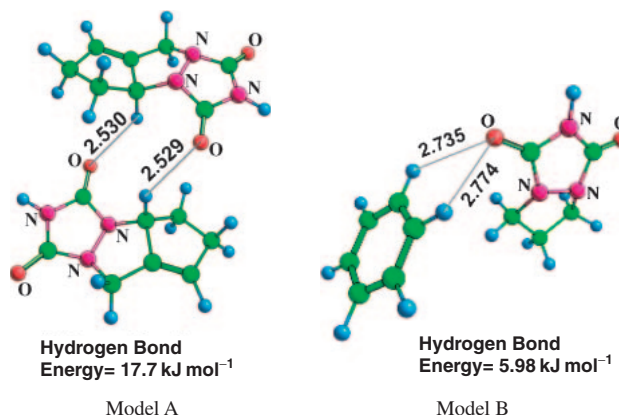

Fig. 6.   B3LYP/6-31G* level optimized model structures A and B constructed from Fragments 1 and 2, respectively (distances in Å).

found in Fragment 1. In the case of Model B, the aryl CH⋯O hydrogen-bond distance (2.774 Å) agreed with the corresponding value (2.769 Å) found in fragment 2, whereas the second aryl CH⋯O hydrogen bond in this model (2.543 Å) was 0.192 Å shorter than the corresponding value found in fragment 2. The interaction energy values between the two dihydrotriazole dione units in Model A and dihydrotriazole dione unit and benzene in Model B were calculated at B3LYP/6-311++G(d,p) level of theory.[18] This level of theory incorporating polarization functions and diffuse functions in the basis set is adequate for estimating the strength of weak intermolecular interactions. From this calculation, the two alkyl CH⋯O=C interaction energy in Model A were found to be 17.7 kJ mol⁻¹ and for the aryl CH⋯O=C interaction energy 5.98 kJ mol⁻¹ in Model B. Since there are two alkyl CH⋯O=C and two aryl CH⋯O=C interactions in the dimer, a value of 29.7 kJ mol⁻¹ energy can be considered as a good estimate for the main stabilizing interaction in the dimer. However, considering the tighter CH⋯O binding in the fragment structures as compared to Model A and B and other minor interactions in the dimer structure, the actual stabilizing interaction is expected to be larger than this value.

Like CH⋯O interaction, the CH⋯N interactions are also important in molecular recognition phenomenon. In the present study, molecule **3** contains six-saturated nitrogen atoms, which would suggest the presence of CH⋯N hydrogen bonds. However, in the crystal packing, no such intermolecular hydrogen bonds were observed. A plausible reason for the lack of such hydrogen bonds is obtained via the following MESP analysis. In Fig. 7, the MESP isosurface of value −78.7 kJ mol⁻¹ is depicted for the optimized geometries of Model A and B. The MESP lobes shown in blue color correspond to the lone pair electron region of the atoms oxygen and nitrogen and the π-region of the arene ring. To further quantify the negative potential, the most negative-valued MESP point in each lobe was also located. As we can see from Fig. 7, the oxygen lone pair regions are two times more negative than the nitrogen lone pair regions. Such high negative potential around the oxygen atom suggests strong electrostatic interaction between the oxygen atoms and the nearby hydrogen atoms, which leads to the preferred formation of CH⋯O hydrogen bonds. The reduction in

the negative potential seen in O1 as compared to O2 in Model A and B is indicative of the electrostatic interaction between heterocycle and the hydrocarbon region. The MESP around O2 in Model A was less negative than that in Model B, which also support the higher interaction energy found in Model A.

It should be noted that for a molecule p-benzoquinone in which the effect of heteroatom or the ring strain is absent, the computed MESP minimum (at B3LYP/6-31* level) was $-163 \, \text{kJ mol}^{-1}$. This result and the MESP analysis of Model A and B suggested that the negative region of the nitrogen atoms was much smaller than those of the oxygen because of the substantial flow of electrons from the nitrogen rich heterocycle to the carbonyl oxygen in **3**. Therefore, though the CO bond is a better hydrogen-bond acceptor than the amide or imide nitrogen atoms, in **3** the presence of the heterocycle further enhances its hydrogen-bonding ability.
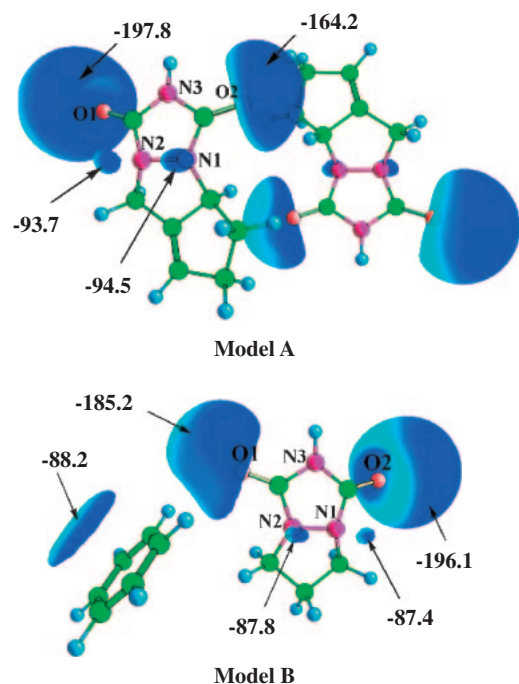

Model A

Model B

Fig. 7. Molecular electrostatic potential (MESP) isosurfaces of value $-78.7 \, \text{kJ mol}^{-1}$ drawn for Model A and B. The depicted values are the most negative-valued point in each MESP lobe in kJ mol^{-1}. The MESP minimum above N3 atom is $-15.5 \, \text{kJ mol}^{-1}$ in Model A and $-14.7 \, \text{kJ mol}^{-1}$ in Model B.

We also attempted to model the interaction between ethyl acetate and the surrounding arene rings given in Fig. 4. The geometry optimized at B3LYP/6-31G* level for this model (Model C) is depicted in Fig. 8 along with the important interatomic distances. The optimized structure showed all the major structural features of the X-ray structure given in Fig. 4. The CH···O hydrogen bonds were reproduced in the calculated structure. However, the weaker CH···π interaction distances were slightly longer than those found in the crystal. It must be noted that to optimize Model C, we did not apply any geometry constraints. Therefore, the good agreement between the X-ray structure and the Model C geometry suggests the importance of the directional nature of the CH···O and CH···π interactions that holds all the molecular units in their respective positions. Interaction energy for the aromatic pocket and ethyl acetate was calculated at B3LYP/6-311++G(d,p) level by subtracting the sum of the single point energies of the ethyl acetate and the rest of the hydrocarbon unit in Model C from the total energy of Model C, and it was determined to be $7.1 \, \text{kJ mol}^{-1}$.

We also analyzed the MESP of Model C without ethyl acetate (the aromatic pocket) and with ethyl acetate. It was found that complexation reduced the negative potential on the arene rings involved in CH···π interaction and also on the arene ring interacting with the ether oxygen (Table 1). For the arene rings involved in CH···π interaction, the maximum reduction in the MESP value was calculated to be $8 \, \text{kJ mol}^{-1}$. On the other hand, in the case of the arene ring interacting with the carbonyl oxygen, the negative MESP was increased by $29 \, \text{kJ mol}^{-1}$. Further, compared to ethyl acetate, in Model C, the negative
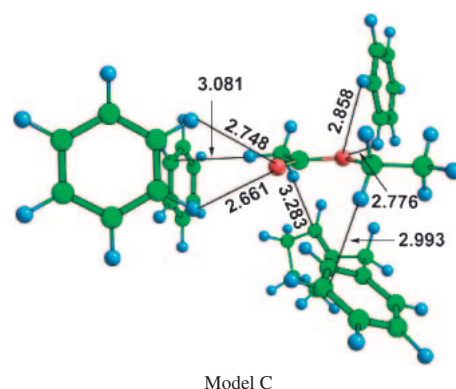

Model C

Fig. 8. B3LYP/6-31G* level optimized structure for Model C. Distances in Å.

Table 1. Most Negative-Valued MESP (in kJ mol^{-1}) on the Aromatic Rings, CC Double Bond on Five-Memberd Ring, and Oxygen Atoms

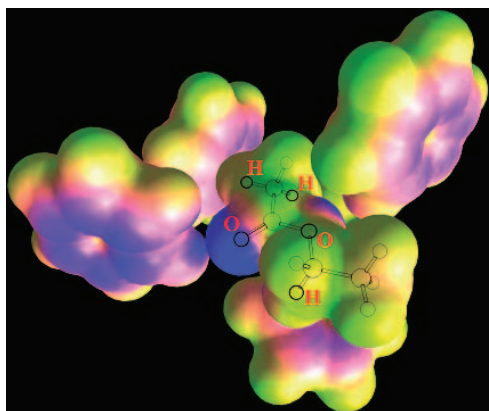| Minimum MESP value on	Model C	Aromatic pocket[a]	Ethyl acetate[a]
CC double bond in the 5-membered ring	−69.5	−77.8	
Arene ring interacting with ethyl CH	−61.5	−69.0	
Arene ring interacting with methyl CH	−74.5	−75.7	
Arene ring interacting with ether O	−62.3	−67.4	
Arene interacting with carbonyl O	−85.8	−56.9	
Ether O	−93.3		−126
Carbonyl O	−179		−210

a) The geometry is taken from Model C.

Fig. 9.   Ethyl acetate trapped inside an aromatic pocket visualized via the MESP painted on the van der Waals surface. Color code (▬▬▬▬) from blue to red is −79 to 289.8 kJ mol⁻¹. The oxygen and hydrogen atoms involved in CH···O and CH···π interactions are also shown.
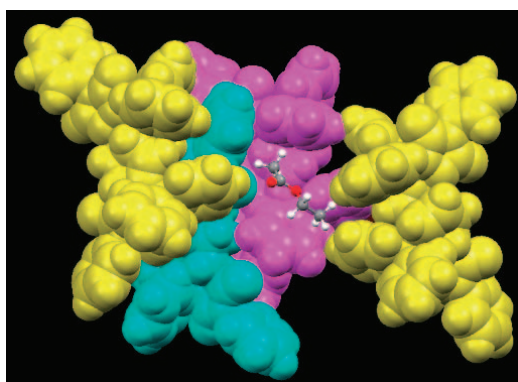
Fig. 10.   PM3 level optimized geometry of (**3···Dimer···3**)··· **Ethyl acetate**. The pair consisting of blue and pink is the dimer. Monomers of **3** interacting with the dimer are in yellow. Ethyl acetate trapped inside the aromatic pocket is shown in ball and stick model.

MESP on the ether oxygen and carbonyl oxygen decreased by 33.1 and 30.6 kJ mol⁻¹, respectively. The substantial changes in the MESP on the carbonyl oxygen and on the arene ring interacting with this carbonyl oxygen as well as the bond length features given in Fig. 8 suggest that the arene CH···O=C interaction is the strongest interaction type in Model C. In Fig. 9, ethyl acetate trapped inside the aromatic pocket is illustrated with MESP painted on the van der Waals surface. The electrostatic interaction of the most negative carbonyl oxygen (in the blue shade) with the arene ring is visible in this figure.

An attempt was made to model the molecular assembly containing dimer of **3**, two monomer of **3** interacting with dimer and ethyl acetate interacting with all the four molecules of **3** at PM3 level. This system contained 414 atoms and was designated as (**3···Dimer···3**)···**Ethyl acetate**. The optimized structure of this system is presented in Fig. 10, which showed good agreement with the X-ray structure. From this structure, the segments (**3···Dimer···3**), (**3···Dimer**), **Dimer**, **3**, and **ethyl acetate** were removed, and their respective heat of formation values were calculated at PM3 level. Based on these heat of formation values, it was found that the interaction energy in

Dimer, (**3···Dimer**), (**3···Dimer···3**), and (**3···Dimer···3**)···**Ethyl acetate** were 35.0, 77, 108, and 138 kJ mol⁻¹, respectively. The dimer interaction energy was in good agreement with the interaction energy predicted based on Model A and B structures at B3LYP/6-31G* level. The total interaction energy of 138 kJ mol⁻¹ found in (**3···Dimer···3**)···**Ethyl acetate** is quite substantial and indicates the importance of the collective strength of all the weaker interactions in forming such host–guest complexes.

Conclusion

The results presented in this study suggested that the packing of molecule **3** in the crystal and its host–guest complexation with ethyl acetate are completely controlled by CH···O and CH···π weak intermolecular interactions. The CH···N type intermolecular interactions were conspicuous by their absence. In terms of MESP, the electron density around the lone pair region of carbonyl oxygen atoms was much higher than that around the nitrogen atoms, suggesting the strong electron donation from the nitrogen atoms to the carbonyl groups. As a result, hydrogen-bond accepting power of carbonyl oxygen was increased. On the other hand, the depletion of electron dencity around nitrogen atoms leads to the loss of CH···N type hydrogen-bond interactions. The molecular modeling studies at the DFT and PM3 levels strongly suggested that the collective strength of CH···O and CH···π weak intermolecular interactions are quite substantial and they play a crucial role in the crystal packing as well as the host–guest complexation.

Experimental

Experimental Procedure for the Synthesis of Compounds 3 and 4.   To a solution of 4-phenyl-3H-2,4,6-triazole-3,5(4H)-dione (**2**) (100 mg, 0.56 mmol) in ethyl acetate (20 mL) at 0 °C, 6,6′-diphenylfulvene (**1**) (65 mg, 0.28 mmol) was added slowly under N_2 atmosphere. The reaction mixture was stirred for 2 h at room temperature. After monitoring the reaction by TLC, the reaction mixture was diluted with water (50 mL) and extracted using ethyl acetate (3 × 50 mL). The combined organic layers were washed with saturated brine solution and dried over anhydrous sodium sulfate. The crude product obtained was purified by silica-gel column chromatography to afford products **3** (84 mg) and **4** (72 mg) in 81% yield (1:1.2). Compound **3** was crystallized from ethyl acetate–hexane mixture to afford colorless crystals. mp: 247 °C.

Compound **3**: Colorless solid, mp, 247 °C. R_f: 0.58 (1:1 hexane/ethyl acetate). IR (Neat) ν_{max}: 3064, 2926, 2857, 1769, 1718, 1600, 1497, 1407, 1280, 1134, 813, 758, 700, 648, 505 cm⁻¹. ¹H NMR (300 MHz, CDCl₃) δ 7.53–7.14 (m, 30H), 6.26 (dd, $J_1 = 2.8$ Hz, $J_2 = 5.6$ Hz, 1H), 5.87 (d, $J = 5.8$ Hz, 1H), 5.04 (d, $J = 8.5$ Hz, 1H), 4.36 (s, 1H), 4.13 (s, 2H), 3.94 (s, 1H), 3.65 (m, 1H). ¹³C NMR (75 MHz, CDCl₃) δ 152.9, 150.7, 150.2, 149.1, 140.6, 140.4, 138.4, 138.0, 134.2, 133.6, 131.4, 130.7, 130.5, 129.8, 129.31, 129.2, 129.0, 128.9, 128.9, 128.4, 128.4, 128.0, 127.9, 127.8, 127.7, 127.1, 126.7, 125.4, 75.2, 64.0, 53.4, 46.4, 41.5, 30.3, 29.6, 14.0. MS (FAB, M + 1): Calcd for $C_{52}H_{38}N_6O_4$: 811.30, Found: 812.04. Elemental analysis calcd for $C_{52}H_{38}N_6O_4$: C, 77.02; H, 4.72; N, 10.36; O, 7.89%. Found: C, 77.04; H, 4.69; N, 10.39; O, 7.88%.

Compound **4**: Light yellow solid, mp, 150 °C. R_f: 0.27 (1:1 hexane/ethyl acetate). IR (Neat) ν_{max}: 3065, 2957, 2855, 1768, 1734, 1597, 1498, 1396, 1283, 1142, 1014, 916, 749, 696, 642,

K. V. Radhakrishnan et al.

Bull. Chem. Soc. Jpn. Vol. 80, No. 3 (2007)   489

Table 2. Summary of Crystallographic Data for Compound **3**

Chemical formula	$C_{52}H_{38}N_6O_4$
Formula weight (M_r)	810.30
Crystal size/mm^3	$0.20 \times 0.16 \times 0.08$
Crystal system	Triclinic
Space group	$P\bar{1}$
$a/\text{Å}$	12.2707(13)
$b/\text{Å}$	13.5989(15)
$c/\text{Å}$	15.4906(17)
$\alpha/°$	71.100(2)
$\beta/°$	73.300(2)
$\gamma/°$	72.169(2)
Z	2
$V/\text{Å}^3$	2276.7(4)
Radiation used $\lambda/\text{Å}$	0.71073
$D_{calcd}/\text{g cm}^{-3}$	1.313
Abs coeff. μ/mm^{-1}	0.087
θ_{max}/deg	28.26
No. of reflections collected	13579
No. of independent reflections	9964
No. of parameters	615
$F(000)$	946
Temp/K	100
GOF on F^2	1.036
$R1/wR2([I > 2\sigma(I)]$	$R1 = 0.0751/0.1961$
$R1/wR2$(all data)	0.1457/0.2384

$508\,\text{cm}^{-1}$. ^{1}H NMR (300 MHz, CDCl$_3$) δ 7.55–7.16 (m, 20H), 7.03 (d, $J = 5.6\,\text{Hz}$, 1H), 6.47–6.45 (m, 1H), 5.56 (s, 1H), 4.73 (s, 1H). ^{13}C NMR (75 MHz, CDCl$_3$) δ 157.4, 155.7, 150.2, 149.5, 138.7, 136.5, 130.9, 130.4, 129.5, 128.9, 128.7, 128.6, 128.5, 128.4, 128.3, 128.29, 128.2, 128.1, 127.8, 127.7, 125.3, 125.2, 125.1, 123.6, 71.8, 62.1, 29.9, 29.2. MS (FAB, M + 1): Calcd for $C_{34}H_{24}N_6O_4$: 581.19, Found: 581.38. Elemental analysis calcd for $C_{34}H_{24}N_6O_4$: C, 70.34; H, 4.17; N, 14.47; O, 11.02%. Found: C, 70.23; H, 4.10; N, 14.58; O, 11.09%.

X-ray Data Collection, Structure Determination, and Refinement.[11] The single-crystal diffraction data were collected on a Bruker AXS Smart Apex CCD diffractometer at 100(2) K. The X-ray generator was operated at 50 kV and 30 mA using Mo Kα radiation. The data was reduced using SAINTPLUS and an empirical absorption correction was applied using the package SADABS. XPREP was used to determine the space group. The crystal structure was solved by direct methods using SHELXS97 and refined by full-matrix least-squares methods using SHELXL97. Molecular and packing diagrams were generated using ORTEP-III and PLATON. All the hydrogen atoms of the compound were set in calculated positions and refined as riding atoms. Details of data collection and refinement are given in Table 2.

CCDC-275653 for compound **3** contains the supplementary crystallographic data for this paper. These data can be obtained free of charge via http://www.ccdc.cam.ac.uk/conts/retrieving. html (or from the Cambridge Crystallographic Data Centre, 12, Union Road, Cambridge, CB2 1EZ, UK; Fax: +44 1223 336033; e-mail: deposit@ccdc.cam.ac.uk).

References

1   a) J. D. Dunitz, A. Gavezzotti, *Angew. Chem., Int. Ed.* **2005**, *44*, 1766. b) G. R. Desiraju, *Acc. Chem. Res.* **2002**, *35*, 565. c) A. Frontera, C. Garau, D. Quinonero, P. Ballester, A. Costa, P. M. Deya, *Org. Lett.* **2003**, *5*, 1135. d) E. A. Meyer, R. K. Castellano, F. Diederich, *Angew. Chem., Int. Ed.* **2003**, *42*, 1210. e) M. Nishio, *Tetrahedron* **2005**, *61*, 6923. f) C. A. Hunter, *Angew. Chem., Int. Ed.* **2004**, *43*, 5310.

2   a) G. A. Jeffrey, *An Introduction to Hydrogen Bonding*, Oxford University Press, New York, **1997**. b) G. R. Desiraju, T. Steiner, *The Weak Hydrogen Bond in Structural Chemistry and Biology*, Oxford University Press, Oxford, **1999**. c) M. Meot-Ner, *Chem. Rev.* **2005**, *105*, 213.

3   T. Steiner, *Angew. Chem., Int. Ed.* **2002**, *41*, 48.

4   a) K. Biradha, *CrystEngComm* **2003**, *5*, 374. b) M. Nishio, *CrystEngComm* **2004**, *6*, 130. c) W. Reckien, S. D. Peyerimhoff, *J. Phys. Chem. A* **2003**, *107*, 9634. d) N. Schultheiss, C. L. Barnes, E. Bosch, *Cryst. Growth Des.* **2003**, *3*, 573. e) L. R. Nassimbeni, *Acc. Chem. Res.* **2003**, *36*, 631. f) V. Klusak, Z. Havlas, L. Rulisek, J. Vondrasek, A. Svatos, *Chem. Biol.* **2003**, *10*, 331. g) R. J. Doerksen, C. Bin, D. H. Liu, G. N. Tew, W. F. DeGrado, M. L. Klein, *Chem. Eur. J.* **2004**, *10*, 5008. h) S. Yohannan, S. Faham, D. Yang, D. Grosfeld, A. K. Chamberlain, J. U. Bowie, *J. Am. Chem. Soc.* **2004**, *126*, 2284. i) V. Spiwok, P. Lipovova, T. Skalova, E. Buchtelova, J. Hasek, B. Kralova, *Carbohydr. Res.* **2004**, *339*, 2275.

5   Y. Umezawa, S. Tsuboyama, H. Takahashi, J. Uzawa, M. Nishio, *Tetrahedron* **1999**, *55*, 10047.

6   a) G. Bhattacharjya, G. Savitha, G. Ramanathan, *CrystEngComm* **2004**, *6*, 233. b) S. Blanco, J. C. Lopez, A. Lesarri, W. Caminati, J. L. Alonso, *ChemPhysChem* **2004**, *5*, 1779. c) R. K. Castellano, *Curr. Org. Chem.* **2004**, *8*, 845. d) A. Cosp, I. Larrosa, J. M. Anglada, J. M. Bofill, P. Romea, F. Urpi, *Org. Lett.* **2003**, *5*, 2809. e) V. Venkatesan, A. Fujii, N. Mikami, *Chem. Phys. Lett.* **2005**, *409*, 57. f) C. Ramos, P. R. Winter, J. A. Stearns, T. S. Zwier, *J. Phys. Chem. A* **2003**, *107*, 10280. g) V. Chandrasekhar, S. Nagendran, S. Bansal, A. W. Cordes, A. Vij, *Organometallics* **2002**, *21*, 3297. h) H. Mansikkamäki, M. Nissinen, K. Rissanen, *Angew. Chem., Int. Ed.* **2004**, *43*, 1243.

7   a) H. Olsen, *Angew. Chem., Int. Ed.* **1982**, *21*, 383. b) B.-C. Hong, A. K. Gupta, M.-F. Wu, J.-H. Liao, *Tetrahedron Lett.* **2004**, *45*, 1663.

8   For [2 + 2], see: a) K. Imafuku, K. Arai, *Synthesis* **1989**, 501. b) L. A. Paquette, J. A. Colapret, D. R. Andrews, *J. Org. Chem.* **1985**, *50*, 201. For [4 + 2] see: c) M. Harre, P. Raddatz, R. Walenta, E. Winterfeldt, *Angew. Chem., Int. Ed.* **1982**, *21*, 480. d) R. Gleiter, O. Borzyk, *Angew. Chem., Int. Ed.* **1995**, *34*, 1001. For [2 + 4], see: e) Y. Himeda, H. Yamataka, I. Ueda, M. Hatanaka, *J. Org. Chem.* **1997**, *62*, 6529. For [6 + 4], see: f) Y. N. Gupta, M. J. Doa, K. N. Houk, *J. Am. Chem. Soc.* **1982**, *104*, 7336. g) Z.-I. Yoshida, M. Shibata, E. Ogino, T. Sugimoto, *Angew. Chem., Int. Ed.* **1985**, *24*, 60. For [6 + 2] and [6 + 3], see: h) B.-C. Hong, Y. J. Shr, J. L. Wu, A. K. Gupta, K. Lin, *Org. Lett.* **2002**, *4*, 2249. i) M. Suda, K. Hafner, *Tetrahedron Lett.* **1977**, *18*, 2453. j) T. C. Wu, K. N. Houk, *J. Am. Chem. Soc.* **1985**, *107*, 5308. k) B.-C. Hong, S. S. Sun, Y. C. Tsai, *J. Org. Chem.* **1997**, *62*, 7717. l) J. Barluenga, S. Martinez, A. L.

Suarez-Sobrino, M. Tomas, *J. Am. Chem. Soc.* **2001**, *123*, 11113. m) K. V. Radhakrishnan, K. Syam Krishnan, M. M. Bhadbhade, G. V. Bhosekar, *Tetrahedron Lett.* **2005**, *46*, 4785, and references cited therein. n) S. K. Krishnan, V. S. Sajisha, S. Anas, C. H. Suresh, M. M. Bhadbhade, G. V. Bhosekar, K. V. Radhakrishnan, *Tetrahedron* **2006**, *62*, 5952.

9   a) R. C. Cookson, S. S. H. Gilani, I. D. R. Stevens, *Tetrahedron Lett.* **1962**, *3*, 615. b) R. C. Gupta, C. M. Raynor, R. J. Stoodley, A. M. Z. Slawin, D. J. Williams, *J. Chem. Soc., Perkin Trans. 1* **1988**, 1773. c) R. C. Gupta, D. S. Larsen, R. J. Stoodley, *J. Chem. Soc., Perkin Trans. 1* **1989**, 739.

10   a) W. H. Pirkle, J. C. Stickler, *Chem. Commun.* **1967**, 760. b) W. Adam, A. Pastor, T. Wirth, *Org. Lett.* **2000**, *2*, 1295, and references cited therein.

11   a) *SMART (V 5.628), SAINT (V 6.45a), XPREP, SHELXTL*, Bruker AXS Inc., Madison, WI, **2004**. b) G. M. Sheldrick, *SHELXL97, Program for Crystal Structure Refinement*, University of Göttingen, Göttingen, Germany, **1997**. c) C. K. Johnson, *ORTEP III, Report ORNL-5138*, Oak Ridge National Laboratory, Oak Ridge, TN, **1976**. d) A. L. Spek, *Acta Crystallogr., Sect. A* **1990**, *46*, C34.

12   a) A. D. Becke, *J. Chem. Phys.* **1993**, *98*, 5648. b) A. D. Becke, *Phys. Rev. A* **1988**, *38*, 3098.

13   C. T. Lee, W. T. Yang, R. G. Parr, *Phys. Rev. B* **1988**, *37*, 785.

14   M. J. Frisch, G. W. Trucks, H. B. Schlegel, G. E. Scuseria, M. A. Robb, J. R. Cheeseman, J. A. Montgomery, Jr., T. Vreven, K. N. Kudin, J. C. Burant, J. M. Millam, S. S. Yengar, J. Tomasi, V. Barone, B. Mennucci, M. Cossi, G. Scalmani, N. Rega, G. A. Petersson, H. Nakatsuji, M. Hada, M. Ehara, K. Toyota, R. Fukuda, J. Hasegawa, M. Ishida, T. Nakajima, Y. Honda, O. Kitao, H. Nakai, M. Klene, X. Li, J. E. Knox, H. P. Hratchian, J. B. Cross, V. Bakken, C. Adamo, J. Jaramillo, R. Gomperts, R. E. Stratmann, O. Yazyev, A. J. Austin, R. Cammi, C. Pomelli, J. W. Ochterski, P. Y. Ayala, K. Morokuma, G. A. Voth, P. Salvador, J. J. Dannenberg, V. G. Zakrzewski, S. Dapprich, A. D. Daniels, M. C. Strain, O. Farkas, D. K. Malick, A. D. Rabuck, K. Raghavachari, J. B. Foresman, J. V. Ortiz, Q. Cui, A. G. Baboul, S. Clifford, J. Cioslowski, B. B. Stefanov, G. Liu, A. Liashenko, P. Piskorz, I. Komaromi, R. L. Martin, D. J. Fox, T. Keith, M. A. Al-Laham, C. Y. Peng, A. Nanayakkara, M. Challacombe, P. M. W. Gill, B. Johnson, W. Chen, M. W. Wong, C. Gonzalez, J. A. Pople, *Gaussian 03, Revision C.02*, Gaussian, Inc., Wallingford CT, **2004**.

15   P. C. Hariharan, J. A. Pople, *Mol. Phys.* **1974**, *27*, 209.

16   J. J. P. Stewart, *J. Comput. Chem.* **1989**, *10*, 209.

17   a) P. Politzer, D. G. Truhlar, *Chemical Applications of Atomic and Molecular Electrostatic Potentials*, Plenum, New York, **1981**. b) S. R. Gadre, R. N. Shirsat, *Electrostatics of Atoms and Molecules*, Universities Press, Hyderabad, **2000**. c) F. S. Dukhovich, M. B. Darkhovskii, *J. Mol. Recognit.* **2003**, *16*, 191. d) A. Boudon, J. Szymoniak, J. R. Chretien, *Eur. J. Med. Chem.* **1988**, *23*, 365. e) C. K. Bagdassarian, V. L. Schramm, S. D. Schwartz, *J. Am. Chem. Soc.* **1996**, *118*, 8825. f) P. Kovacic, L. P. G. Wakelin, *Anti-Cancer Drug Des.* **2001**, *16*, 175. g) F. J. Luque, M. Orozco, P. K. Bhadane, S. R. Gadre, *J. Phys. Chem.* **1993**, *97*, 9380. h) S. R. Gadre, K. Babu, A. P. Rendell, *J. Phys. Chem. A* **2000**, *104*, 8976. i) C. H. Suresh, S. R. Gadre, *J. Org. Chem.* **1999**, *64*, 2505. j) C. H. Suresh, N. Koga, S. R. Gadre, *J. Org. Chem.* **2001**, *66*, 6883. k) C. H. Suresh, N. Koga, *J. Am. Chem. Soc.* **2002**, *124*, 1790. l) P. Politzer, P. R. Laurence, K. Jayasuriya, *Environ. Health Perspect.* **1985**, *61*, 191. m) J. S. Murray, S. Ranganathan, P. Politzer, *J. Org. Chem.* **1991**, *56*, 3734.

18   R. C. Smith, C. R. Bodner, M. J. Earl, N. C. Sears, N. E. Hill, L. M. Bishop, N. Sizemore, D. T. Hehemann, J. J. Bohn, J. D. Protasiewicz, *J. Organomet. Chem.* **2005**, *690*, 477.